Available online at www.sciencedirect.com
SCIENCE DIRECT®
Pergamon
Acta Materialia 51 (2003) 5529–5543
Acta MATERIALIA
www.actamat-journals.com

Twinning and detwinning of ⟨0 1 1⟩ type II twin in shape memory alloy

Yong Liu [a,*], Z.L. Xie [b]

[a] *School of Mechanical and Production Engineering, Nanyang Technological University, Singapore*
[b] *School of Materials Engineering, Nanyang Technological University, Singapore*

Received 18 June 2003; received in revised form 17 July 2003; accepted 21 July 2003

Abstract

⟨0 1 1⟩ type II twin is a major twinning mode frequently observed in NiTi shape memory alloy. Its response to applied stresses is responsible for various inelastic deformation processes. In order to predict the shape recovery characteristic under various conditions, it is of primary importance to predict the martensite detwinning characteristic prior to the reverse transformation. However, due to its irrational nature, the type II twin plane is not as easily comprehensible as that of other types of twins and a strong disagreement exists over the nature of the twin boundary. In the present research, the ⟨0 1 1⟩ type II twin boundary before and after deformation was investigated. A complete model of ⟨0 1 1⟩ type II twin plane and its role in the detwinning process are proposed which can be used to account for the various experimental observations.

Keywords: SMA; HREM; Twinning; Detwinning; Interface

1. Introduction

Twinning and detwinning are important microstructural processes partially responsible for shape memory effect in both shape memory alloys (SMAs) and magnetic shape memory materials. In the case of thermally induced shape memory effect, NiTi SMAs have attracted the most attention due to their properties superior over other classes of SMAs. The unique combination of properties are shape memory effect, superelasticity, high damping capacity, excellent biocompatibility and fatigue resistance, etc. These properties lead to their successful applications in various engineering practices [1–6]. Regardless the successful applications, some fundamental problems still remain unsolved, which retard further applications of these materials. One of the major problems is that both the mechanical and the thermomechanical characteristics of SMAs cannot be satisfactorily predicted. In order to predict the response of SMAs as a function of various factors namely temperature, loading mode, pre-strain, texture distribution, cyclic degradation, etc., a great effort has been made both experimentally and theoretically. However, the theoretical work conducted so far is unable to provide satis-

* Corresponding author. Tel./fax: +65-679-04951.
E-mail address: mliuy@ntu.edu.sg (Y. Liu).

1359-6454/$30.00
doi:10.1016/S1359-6454(03)00417-8

factory predication of both the pure mechanical behaviour of SMAs and their shape recovery as a function of loading mode, pre-strain and texture distribution. From our point of view, in order to accurately predict the shape recovery process, the details in detwinning should be taken into consideration. It is known that the deformation associated with detwinning is recoverable while that associated with dislocation processes is irrecoverable. If we are able to predict the detwinning magnitude as a function of the influencing factors, we will have a good chance to predict the subsequent shape recovery process. Thus, a complete understanding of the detwinning mechanism is a prerequisite.

In NiTi SMAs, three types of twins are frequently observed, namely, $\langle 0\,1\,1\rangle$ type II twin, $(1\,1\,\bar{1})$ type I twin and $(0\,0\,1)$ or $(1\,0\,0)$ compound twins [7–9]. Among them, the $\langle 0\,1\,1\rangle$ type II twin is the main lattice twin and is responsible for various inelastic deformation processes. Different from type I and compound twins, the $\langle 0\,1\,1\rangle$ type II twin was found to have an irrational twin plane. Although some efforts have been made, the nature of $\langle 0\,1\,1\rangle$ type II twin boundary is still not clearly understood and a strong disagreement exists. This further adds difficulties to the understanding of its detwinning mechanism in atomic scale.

Christian [10] has proposed that, in order to reduce the total interfacial strain energy, the irrational twin plane consists of ledges of low-index rational plane that are connected by steps of atomic dimension parallel to another low-index plane. Based on this idea, Knowles [11] has tried to experimentally determine the structure of $\langle 0\,1\,1\rangle$ type II twin plane by using HREM along the $[1\,1\,2]_A//[1\,\bar{2}\,1]_B$ zones, and concluded that the irrational twin boundary consists of ledges of $(1\,1\,\bar{1})$ plane and steps parallel to $(0\,1\,\bar{1})$ plane. Unfortunately, his work did not provide clearly resoluble atomic images and hence was not very convincing. Based on their HREM observations from both [0 1 1] and the $[1\,1\,2]_A//[\bar{1}\,2\,1]_B$ zones, Nishida et al. [12] argued about the existence of $(1\,1\,\bar{1})$ ledges along the irrational twin plane. As will be shown in this study, both the $[1\,1\,2]_A//[\bar{1}\,2\,1]_B$ and the [0 1 1] directions are not ideal directions to observe the $\langle 0\,1\,1\rangle$ type II twin plane. Thus, corresponding observations are unable to provide convincing evidence either supporting or opposing the model of Christian.

In the present work, the $\langle 0\,1\,1\rangle$ type II twin boundary is carefully studied along the $[1\,0\,1]_A//[\bar{1}\,1\,0]_B$ zones that are the lowest index directions in the $(1\,1\,\bar{1})$ plane besides [0 1 1] direction. Using crystallographic data reported [13], the crystal structure of NiTi $\langle 0\,1\,1\rangle$ type II twin is constructed and is further compared to the present observations and the observations reported by Knowles [11] and Nishida et al. [12]. As a result, a clear picture is obtained on the $\langle 0\,1\,1\rangle$ type II twin plane and its role in the detwinning process. This understanding is useful for the accurate prediction of the shape recovery process in NiTi SMAs.

2. Experimental procedures

A near-equiatomic binary NiTi bar and a NiTi rolled sheet were used in the present work. Samples were annealed at 600 °C for 30 min followed by water quench to room temperature. This annealing treatment enables a complete martensitic structure at room temperature [14,15]. The martensite twins before and after deformation were studied using transmission electron microscope (TEM).

TEM observations were carried out on a Philips CM200 (FEG) microscope operated at 200 kV, using a side-entry type double-tilt specimen stage. Samples for TEM observations were cut using a low speed diamond saw. Thin foils were prepared by first mechanical grinding to about 100 μm and then electropolishing using a twin-jet method, at around −30 °C and in an electrolyte of nitric acid and methanol, 1:3 in volume. The martensite crystal structure and lattice twins were constructed using the crystallographic data listed in Table 1 [13].

3. Results and discussion

3.1. Crystal structure of martensite and $\langle 0\,1\,1\rangle$ type II twin in NiTi

Since the discovery of the shape memory effect in NiTi alloy, a number of investigations on the

Table 1
Crystallographic data and atomic parameters of NiTi martensite

a = 2.885 Å, b = 4.12 Å, c = 4.622 Å, β = 96.8°				
Space group $P2_1/m$, no. 11				
Ni	2*e*	x = 0.0525	y = 1/4	z = 0.693
Ti	2*e*	x = 0.4726	y = 1/4	z = 0.221

Table 2
Direction pairs of ⟨0 1 1⟩ type II twin that lie in the (1 1 $\bar{1}$) and (3 4 $\bar{4}$) planes

Direction pairs of ⟨0 1 1⟩ type II twin that lie in the (1 1 $\bar{1}$) plane		
Zone axes in (1 1 $\bar{1}$) plane	Angular difference (°)	Angle away from [0 1 1] (°)
$[0\ 1\ 1]_A//[0\ \bar{1}\ 1]_B$	0.0	0
$[1\ 3\ 4]_A//[\bar{1}\ 4\ 3]_B$	0.1	
$[1\ 2\ 3]_A//[\bar{1}\ 3\ 2]_B$	0.2	
$[1\ 1\ 2]_A//[\bar{1}\ 2\ 1]_B$	0.5	~23
$[2\ 1\ 3]_A//[\bar{2}\ 3\ 1]_B$	0.8	
$[3\ 1\ 4]_A//[\bar{3}\ 4\ 1]_B$	1.07	
$[1\ 0\ 1]_A//[\bar{1}\ 1\ 0]_B$	1.8	~52
$[4\ \bar{1}\ 3]_A//[\bar{4}\ 3\ \bar{1}]_B$	2.4	
$[3\ \bar{1}\ 2]_A//[\bar{3}\ 2\ \bar{1}]_B$	2.6	
$[2\ \bar{1}\ 1]_A//[\bar{2}\ 1\ \bar{1}]_B$	2.8	~90
Direction pairs of ⟨0 1 1⟩ type II twins that lie in (3 4 $\bar{4}$) plane		
Zone axes in (3 4 $\bar{4}$)	Angular difference (°)	Angle away from [0 1 1] (°)
$[\bar{0}\ 1\ 1]_A//[0\ 1\ \bar{1}]_B$	0.0	
$[\bar{4}\ 3\ 0]_A//[\bar{4}\ 0\ 3]_B$	0.2	~57
$[4\ \bar{1}\ 2]_A//[\bar{4}\ 2\ \bar{1}]_B$	0.3	~78

crystal structure of NiTi martensite have been reported [8,13,16,17]. The NiTi martensite is found to have a B19′ monoclinic unit cell. Although the atomic parameters of NiTi martensite differ slightly among results reported by different researchers, a general agreement has been reached on the lattice parameters of martensite. The crystallographic data reported by Michal and Sinclair [13] fit well with our experimental results [18], and thus are used to construct the crystal structure in the present study. Fig. 1a is the B19′ monoclinic unit cell of NiTi martensite in which the positions of Ni and Ti atoms are indicated. Figs. 1b and 1c is the crystal structures viewed from [1 0 0] and [0 1 0] directions, respectively.

As reported by Knowles and Smith [7], the ⟨0 1 1⟩ type II twin consists of two martensite variants related to each other by a 180° rotational symmetry about [0 1 1] direction. The twinning elements of the ⟨0 1 1⟩ type II twin are as follows: twin plane K_1 = (0.7205 1 $\bar{1}$), shear direction η_1 = [0 1 1], K_2 = (0 1 1) and η_2 = [1.5727 1 $\bar{1}$]. The irrational twin plane is observed to have an angle of about 10 ± 2° away from (1 1 $\bar{1}$) towards (0 1 $\bar{1}$) [7].

The crystallographic orientation relationship of ⟨0 1 1⟩ type II twin can be presented clearly in the stereographic projections shown in Fig. 2. Fig. 2a is the [0 1 1] stereogram of one martensite variant (variant A), where the trace of (1 1 $\bar{1}$) plane and

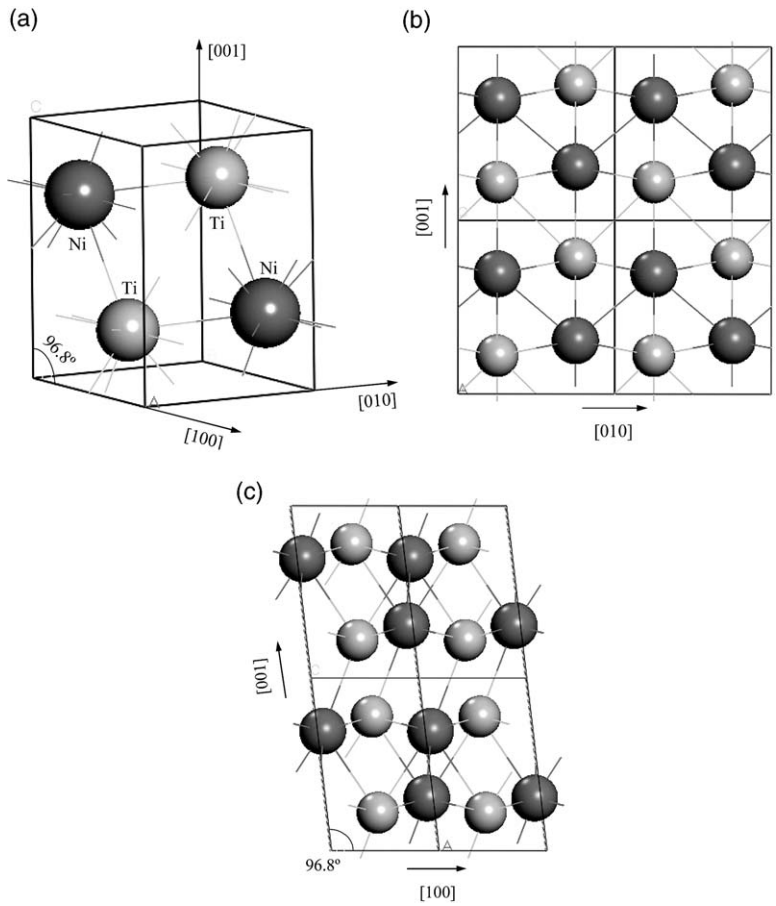

Fig. 1. The B19′ monoclinic unit cell of NiTi martensite (a). Crystal structure of NiTi martensite viewed along [1 0 0] (b) and [0 1 0] (c). ○ Ti, ● Ni.

the directions that lie in this plane are indicated. Fig. 2b shows the orientation relationship of two martensite variants, A and B, having ⟨0 1 1⟩ type II twin relation, where the orientation of variant B is obtained by rotating the stereogram in Fig. 2a by 180° about [0 1 1]. The directions in the two variants that are nearly parallel to each other and are lying in (1 1 $\bar{1}$) plane are listed in Table 2, where subscripts A and B refer to the neighbouring variants A and B, respectively. In addition to (1 1 $\bar{1}$) plane, the trace of (3 4 $\bar{4}$) plane and the directions lying in this plane are also indicated in Fig. 2. The (3 4 $\bar{4}$) (or (0.75 1 $\bar{1}$)) plane is a rational plane that is most close to the irrational twin plane of (0.7205 1 $\bar{1}$). (0.75 1 $\bar{1}$) has about 8.86° away from (1 1 $\bar{1}$) plane, while the angle between (0.7205 1 $\bar{1}$) and (1 1 $\bar{1}$) is about 10.06°.

3.2. HREM observations of ⟨0 1 1⟩ type II twin plane

Knowles [11] and Nishida et al. [12] have tried to experimentally determine the structure of ⟨0 1 1⟩ type II twin plane by using HREM along either [0 1 1] direction or $[1\ 1\ 2]_A // [\bar{1}\ 2\ 1]_B$ directions. In order to clearly observe the twin boundary, it is preferable to observe it along a zone axis that contains (1 1 $\bar{1}$) plane and has the lowest index (except [0 1 1] zone). Among the zones listed in Table 2 and shown in Fig. 2, $[1\ 0\ 1]_A // [\bar{1}\ 1\ 0]_B$ direction

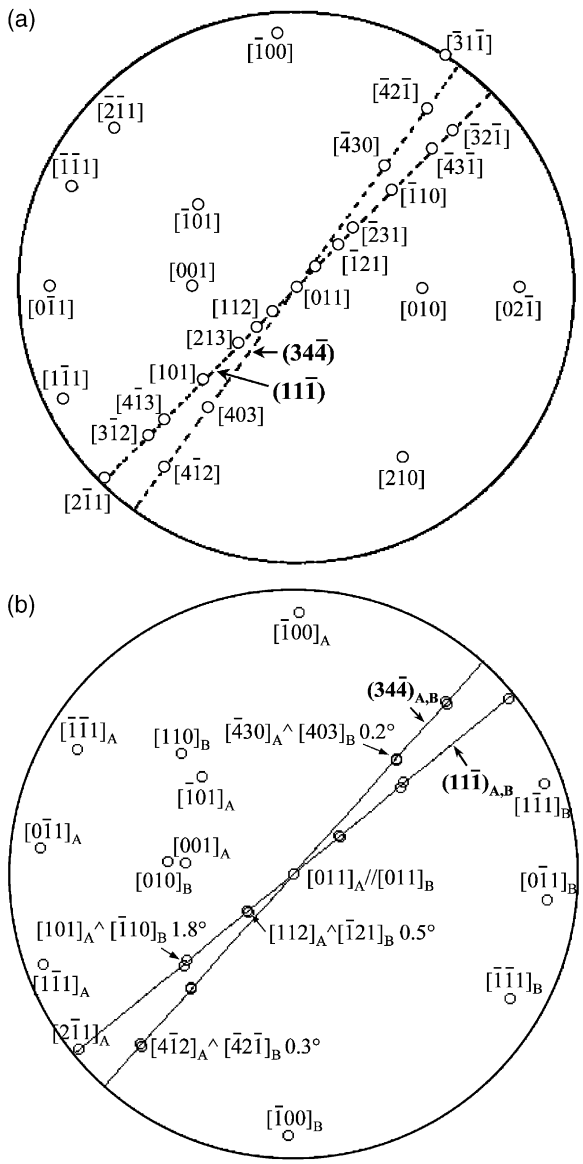

Fig. 2. [0 1 1] stereographic projections of B19' martensite showing the crystallographic orientation relationship of ⟨0 1 1⟩ type II twin. (a) Single martensite variant. (b) Twinned martensite variants having 180° rotational symmetry about [0 1 1].

pair is the best choice for obtaining clearly resoluble atomic image of twin boundary. Thus, in the present research, the ⟨0 1 1⟩ type II twin plane is studied along these directions by using HREM.

Figs. 3a and 4a are two examples of HREM image of ⟨0 1 1⟩ type II twin boundary observed along $[1\,0\,1]_A//[\bar{1}\,1\,0]_B$ directions. Fig. 3a shows a smooth and clear twin boundary. Atomic planes are connected coherently across the boundary and no high strain contrast is visible. After carefully filtering away the noise of the HREM images, the inverse fast Fourier transform (IFFT) images reveal more clearly the atomic configuration of the twin boundary as shown in Figs. 3b and 4b. By carefully drawing parallel lines along the traces of the atomic planes in each variant, the twin boundary can be identified by connecting the intersections of these lines. Fig. 3b shows clearly that the twin boundary consists of $(1\,1\,\bar{1})$ ledges that are connected by steps of atomic dimension.

Different from that shown in Fig. 3a, the twin boundary in Fig. 4a is not a sharp interface. Instead, it is a transition layer and a strain contrast exists along the boundary. It can be seen in Fig. 4b that, although there is a transition layer in between the two variants, the twin boundary is still composed of $(1\,1\,\bar{1})$ ledges. Both sharp interface and transition layer between two martensite variants are frequently observed in the present research. It is known that, as viewed from $[1\,0\,1]_A//[\bar{1}\,1\,0]_B$ directions, the $(0.7205\,1\,\bar{1})$ boundary is a projected area having overlapped region between two variants. Thus, a transition layer may be observed along the variant boundary when the thickness of the observed area is great.

3.3. Model of ⟨0 1 1⟩ type II twin plane

To further understand the atomic accommodation along the irrational twin plane, the atomic structure of ⟨0 1 1⟩ type II twin is constructed. The B19′ martensite is cleaved into two variants having cleaved surfaces parallel to $(3\,4\,\bar{4})$, where the rational plane $(3\,4\,\bar{4})$ or $(0.75\,1\,\bar{1})$ is used to approximate the irrational plane $(0.7205\,1\,\bar{1})$. The crystallographic orientation relationship of ⟨0 1 1⟩ type II twin is shown in Fig. 5a, i.e., $(0.75\,1\,\bar{1})_A//(0.75\,1\,\bar{1})_B$, $[0\,1\,1]_A//[0\,1\,1]_B$, and the two variants have a 180° rotational symmetry about [0 1 1]. As shown in Fig. 5a, the $(0.75\,1\,\bar{1})$ plane is composed of ledges of $(1\,1\,\bar{1})$ plane and steps in (1 1 1) or (0 1 1) plane, which agrees well with the model proposed by Christian [10] and Knowles [11]. It can be clearly seen that the interface

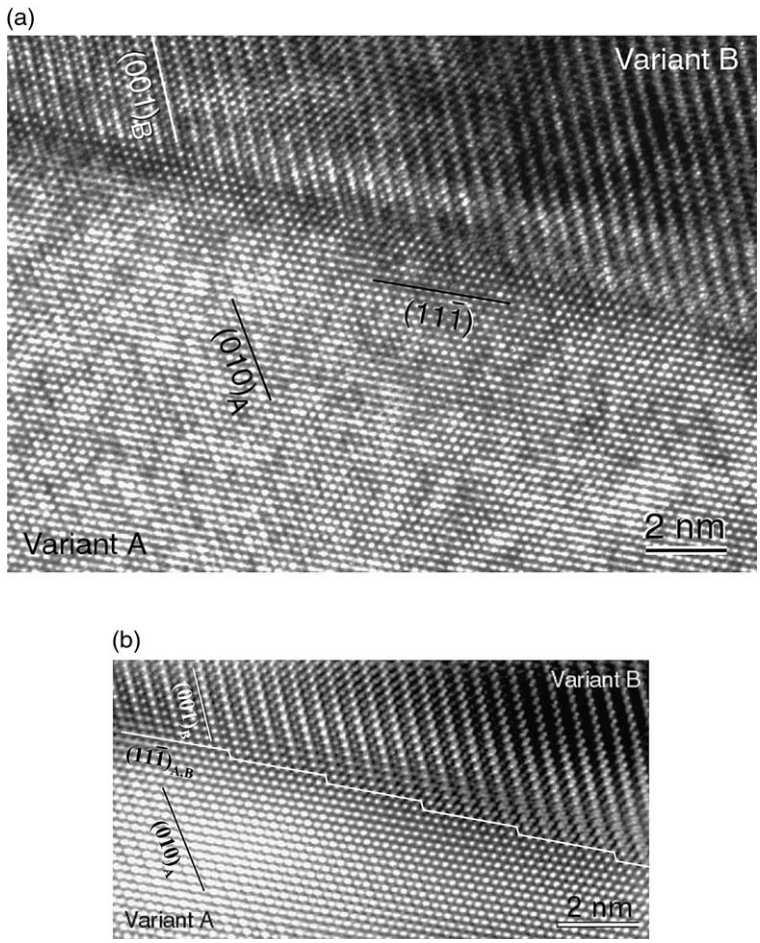

Fig. 3. HREM image of ⟨0 1 1⟩ type II twin boundary (a) and its corresponding IFFT image (b). $\mathbf{B}//[1\,0\,1]_A//[\bar{1}\,1\,0]_B$.

between segments of the two variants is actually $(1\,1\,\bar{1})$ plane. Figs. 5b and 5c further illustrate the atomic arrangement of the two neighbouring variants on the $(1\,1\,\bar{1})$ plane, as viewed from the normal direction of $(1\,1\,\bar{1})$. Since the two martensite variants are actually bonded by $(1\,1\,\bar{1})$ plane, knowing atomic arrangement on this plane is important for understanding the detwinning of the type II twin. As shown in Table 2, the $[2\,\bar{1}\,1]_A$ and $[2\,1\,\bar{1}]_B$ directions are nearly parallel to each other and they are nearly normal to the shear direction $[0\,1\,1]_{A,B}$.

Fig. 6 shows the constructed ⟨0 1 1⟩ type II twin. The two variants look identical when they are viewed along [0 1 1] direction (Fig. 6a). Since the $(0.7205\,1\,\bar{1})$ twin plane, the $(1\,1\,1)$ ledges and $(1\,\bar{1}\,1)$ steps are all in edge-on direction when viewed along the [0 1 1] direction, the twin boundary cannot be easily identified. This might explain why Nishida et al. [12] did not observe distinguished $(1\,1\,\bar{1})$ ledges along this direction. When viewed along $[2\,\bar{1}\,1]_A//[2\,1\,\bar{1}]_B$ direction pair (Fig. 6b), the two variants are related to each other by a reflection symmetry with respect to $(1\,\bar{1}\,1)$ plane. Because the shear plane $(1\,\bar{1}\,1)$ is not normal to $(1\,1\,\bar{1})$, we may call this reflection symmetry a pseudo-mirror-plane symmetry. The corresponding simulated electron diffraction patterns in Fig. 6c,d agrees well with the patterns experimentally observed [7]. It confirms the 180° rotational symmetry about [0 1 1] and the pseudo-$(1\,1\,\bar{1})$-mirror-plane symmetry, providing supporting evi-

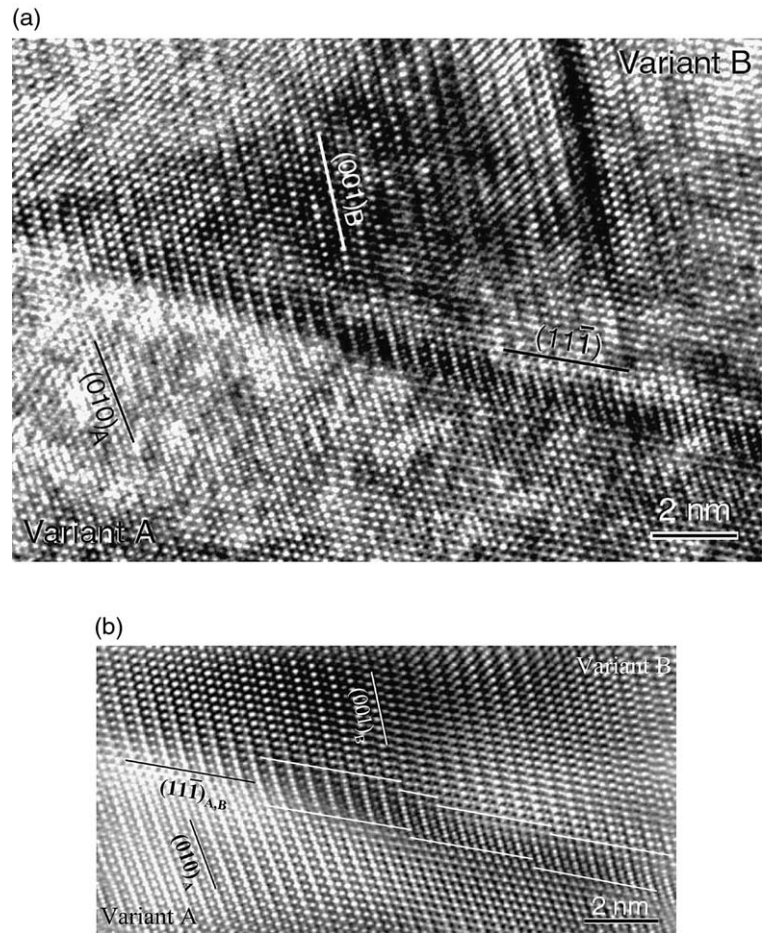

Fig. 4. HREM image of ⟨0 1 1⟩ type II twin boundary (a) and its corresponding IFFT image (b). **B**//$[1\,0\,1]_A$//$[\bar{1}\,1\,0]_B$.

dence on that the constructed ⟨0 1 1⟩ type II twin model closely reflects the reality.

Fig. 7a presents the atomic structure of ⟨0 1 1⟩ type II twin as viewed from $[1\,1\,2]_A$//$[\bar{1}\,2\,1]_B$. As can be seen, the atomic arrangements of the two variants are not significantly different, thus the variant boundary and the (1 1 $\bar{1}$) ledges are not easily visible. Most importantly, when viewed along this direction pair, the distance between the atoms or the atomic columns is too short to obtain a clearly resoluble HREM atomic image. Thus, although both Knowles [11] and Nishida et al. [12] have tried to observe the ⟨0 1 1⟩ type II twin plane along this direction pair, they reached contradictory conclusions.

Fig. 7b presents the constructed ⟨0 1 1⟩ type II twin viewed along $[1\,0\,1]_A$//$[\bar{1}\,1\,0]_B$ zones. The irrational plane is a projected area as shown by the dashed lines, while the (1 1 $\bar{1}$) plane, $(0\,1\,0)_A$ and $(0\,0\,1)_B$ are all in edge-on direction. The twin boundary can now be visualised more clearly. The constructed twin model fits well with the experimental observations (Figs. 3 and 4). The simulated electron diffraction pattern (Fig. 7c) of the constructed lattice twin fits well with the electron diffraction pattern (Fig. 7d) of the observed ⟨0 1 1⟩ type II twin (Fig. 3a).

Based on our observations and analysis, the ⟨0 1 1⟩ type II twin can be further schematically illustrated in Fig. 8. It shows that the irrational plane of (0.7205 1 $\bar{1}$) is merely an overall variant boundary in microscopic scale (micrometers), and

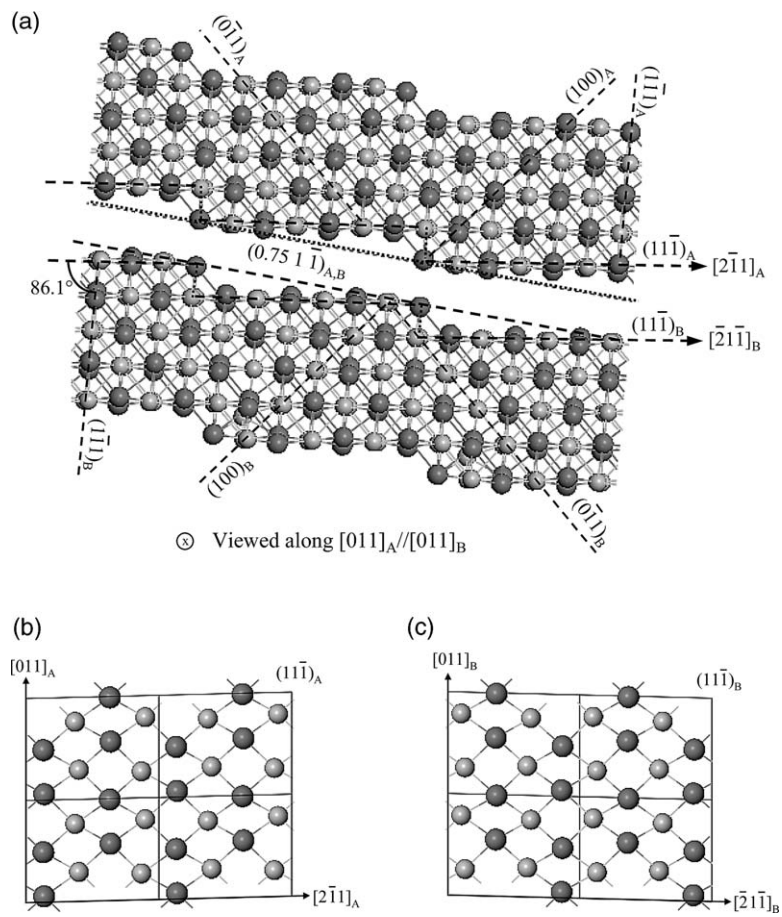

Fig. 5. Crystallographic orientation relationship of two martensite variants of ⟨0 1 1⟩ type II twin. Rational plane (0.75 1 $\bar{1}$) is used to approximate the irrational twin plane (0.7205 1 $\bar{1}$). (a) When viewed along the [0 1 1] shear direction, the variant boundary is composed of (1 1 $\bar{1}$) ledges and (1 1 1) steps. The atomic configuration on (1 1 1) plane of variant A (b) and variant B (c). ○ Ti, ● Ni.

is composed of atomic scale (nanometers) ledges of (1 1 $\bar{1}$) plane and steps of (1 $\bar{1}$ 1) plane. In addition to the 180° rotational symmetry about [0 1 1] direction, the two martensite variants have a pseudo-mirror-plane symmetry with respect to (1 1 $\bar{1}$) plane. In Fig. 8, the relation among the irrational (0.7205 1 $\bar{1}$) twin plane, the rational (1 1 $\bar{1}$) twin plane, the (1 $\bar{1}$ 1) shear plane, the (0 1 1) K_2 plane, and the [0 1 1] shear direction can be easily visualized. Consider only the atomic shear in (1 1 $\bar{1}$) plane, the shear strain can be calculated ($\gamma = 2\times\tan 7.856°$) to be 0.276, which is close to the reported value of 0.2804 [7].

3.4. Detwinning model of ⟨0 1 1⟩ type II twin

It has shown that the ⟨0 1 1⟩ type II twin plays a critical role in controlling the deformation mechanism of NiTi martensite [14,15]. By using an optical microscope, Miyazaki et al. [19] have studied the coalescence of martensite variants under deformation. By recording the surface morphology change during loading, they observed that the self-accommodated martensite variants in a triangular shape disappeared and only one martensite variant existed after the deformation. They further proposed that the coalescence of martensite variants

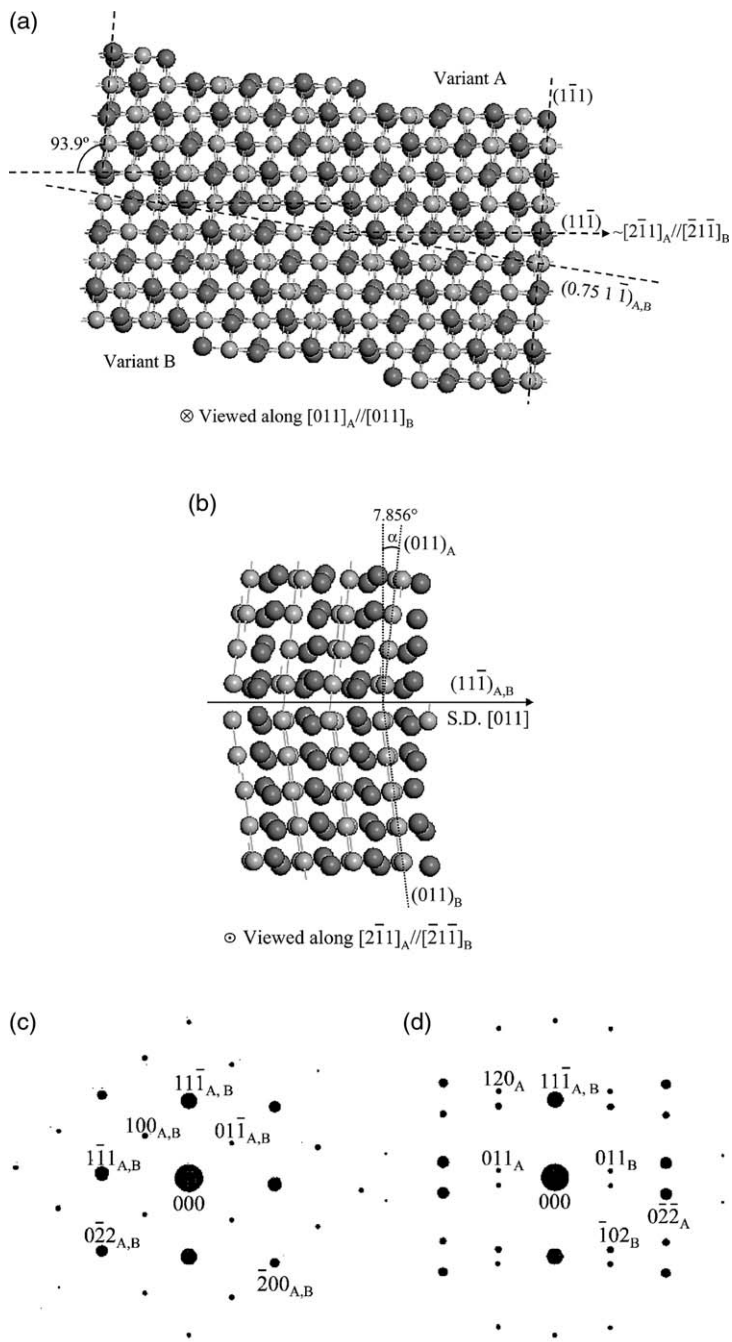

Fig. 6. Atomic structure of $\langle 0\ 1\ 1\rangle$ type II twin as viewed along $[0\ 1\ 1]_{A,B}$ (a) and $[2\ \bar{1}\ 1]_A//[\bar{2}\ 1\ \bar{1}]_B$ (b). Simulated electron diffraction patterns (c) and (d) correspond to structures in (a) and (b), respectively. ○ Ti, ● Ni.

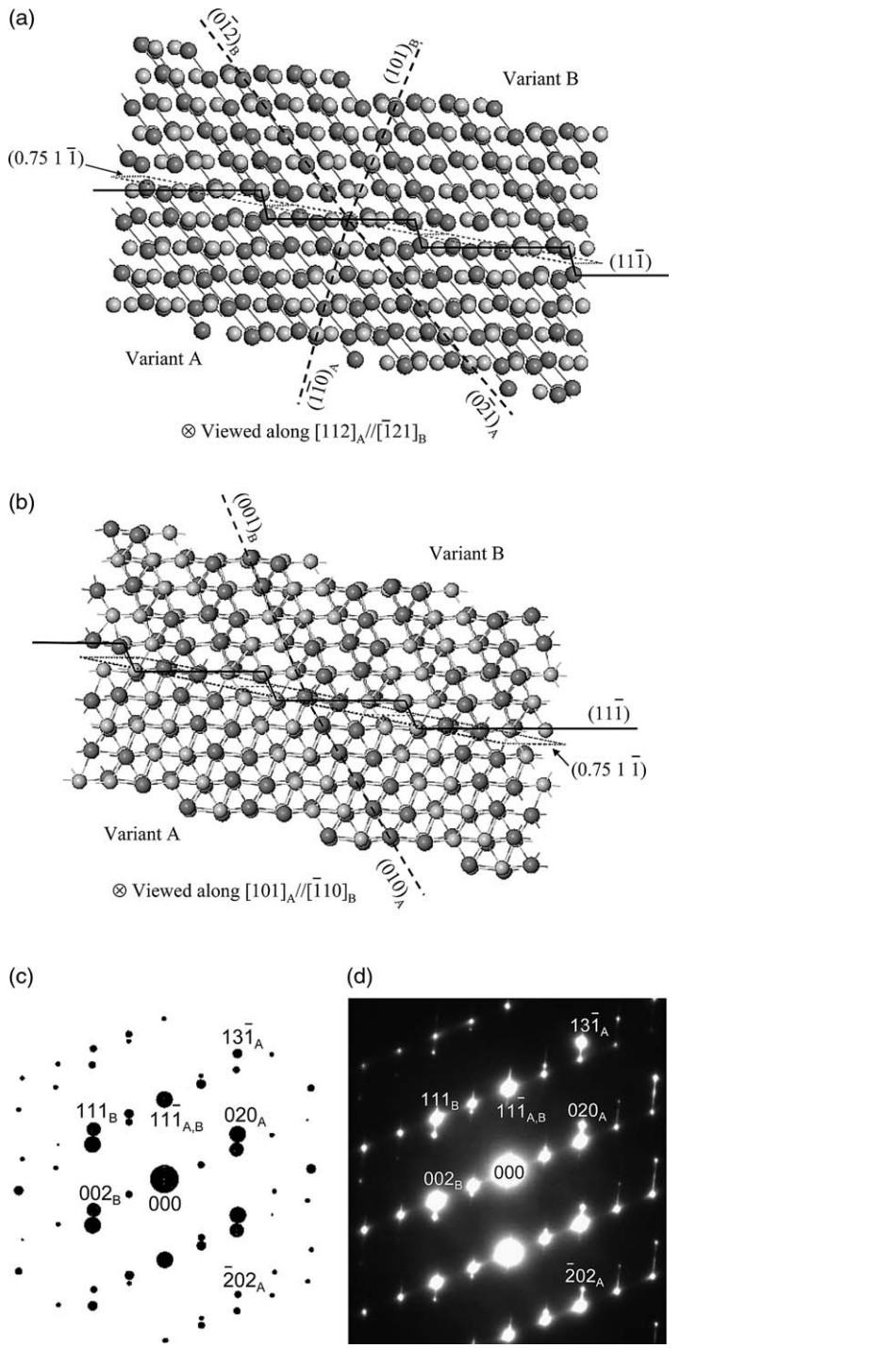

Fig. 7. Crystal structure of ⟨0 1 1⟩ type II twin as viewed along $[1\ 1\ 2]_A//[\bar{1}\ 2\ 1]_B$ (a) and $[1\ 0\ 1]_A//[\bar{1}\ 1\ 0]_B$ (b). Variant boundary is composed of $(1\ 1\ \bar{1})$ ledges and is a projected area between the two variants. Simulated electron diffraction pattern (c) corresponding to structure in (b) fits well with the observed diffraction pattern (d) of the area in Fig. 3a. ○ Ti, ● Ni.

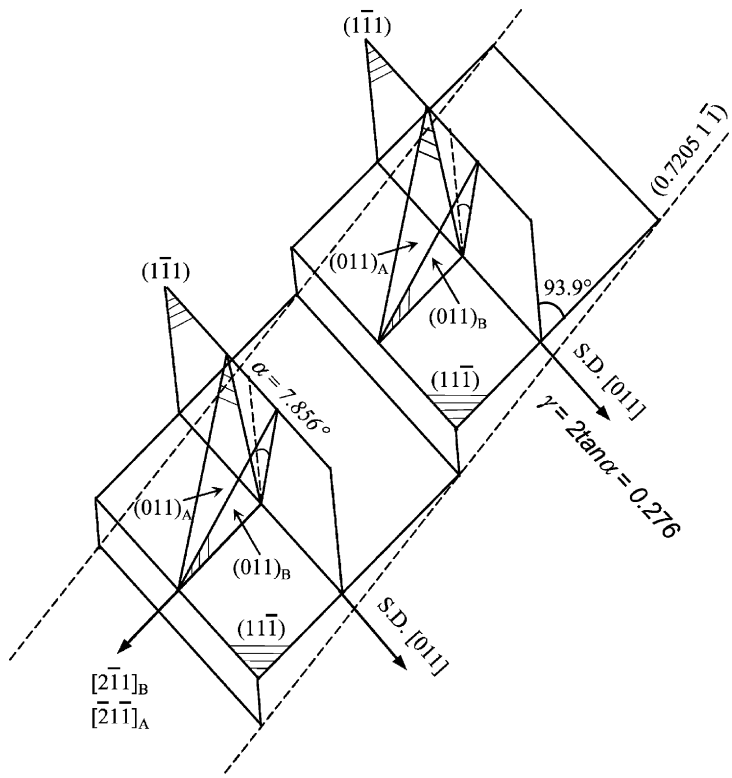

Fig. 8. Schematic illustration of ⟨0 1 1⟩ type II twin. Relation between irrational twin plane (0.7205 1 $\bar{1}$), rational twin plane (1 1 $\bar{1}$), shear plane (1 $\bar{1}$ 1), (0 1 1) K_2 plane, and shear direction [0 1 1] is highlighted. The ⟨0 1 1⟩ type II twin has an overall 180° rotational symmetry about [0 1 1] and a pseudo-mirror-plane symmetry with respect to each ledge of (1 1 $\bar{1}$) plane.

was through the movement of (0.72 1 $\bar{1}$) and ($\overline{0.72}$ 1 1) planes. Such "macroscopic" observation has provided important information on the detwinning of martensite and the proposed interfacial movement is still valid. Nevertheless, optical microscopic observation is unable to provide atomic-scaled understanding on how the (0.72 1 $\bar{1}$) plane migrate during loading, which can only be achieved through the crystallographic analysis combining with the confirmations from the atomically resoluble observations.

It was found that the detwinning of NiTi martensite is anisotropic with respective to deformation mode [20,21] and texture orientation [14]. Recently, Sehitoglu and colleagues have made efforts to understand the shape recovery anisotropy with respect to the loading mode and crystal orientation by using NiTi single crystals. The observed shape recovery magnitude was proposed to be partially related to the detwinning process [22,23]. In order to theoretically predict the detwinning magnitude of ⟨0 1 1⟩ type II twin, its atomistic detwinning mechanism is yet to be established.

Lattice twins having mirror plane symmetry can form through homogeneous shear along the shear direction in the rational twin plane [24]. This model has long been used to explain the formation of compound twin upon deformation, and may also be valid to explain the detwinning of these twins under applied stress. Present observations show that the type II twin plane is not "atomically" irrational (Figs. 3 and 4), it consists of ledges of rational plane. According to the model proposed (Fig. 8), we can reasonably explain that the detwinning of ⟨0 1 1⟩ type II twin is achieved through atomic shear on the rational (1 1 $\bar{1}$) plane along [0 $\underline{1}$ 1] shear direction, where the shear plane is (1 $\underline{\bar{1}}$ 1). Such detwinning mechanism can be sche-

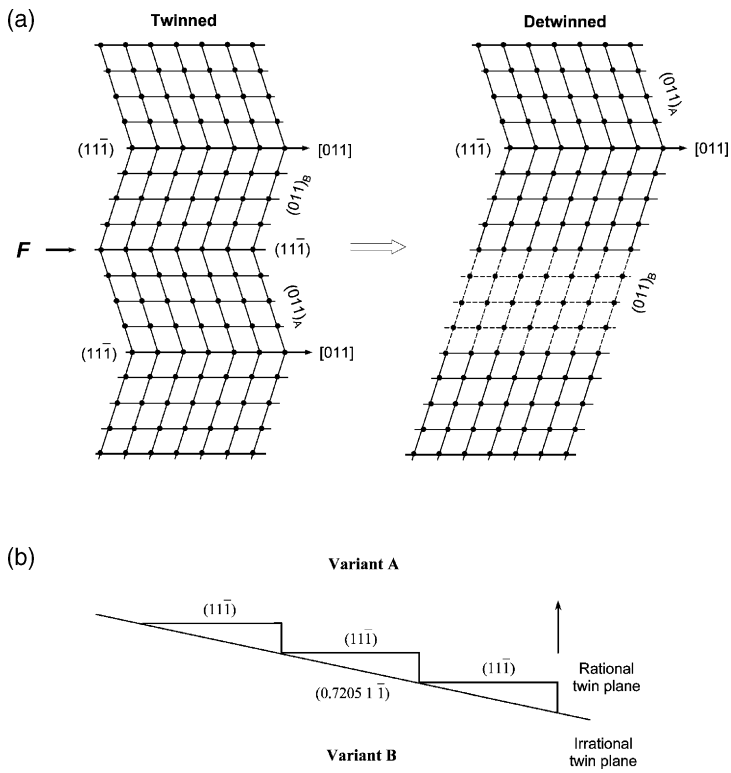

Fig. 9. Schematic two-dimensional representation of the detwinning mechanism of ⟨0 1 1⟩ type II twin. (a) Atomic shear on (1 1 $\bar{1}$) plane along [0 1 $\bar{1}$] direction leads to the advancement of the (1 1 $\bar{1}$) ledges (viewed along $[2\ \bar{1}\ 1]_A$//$[\bar{2}\ 1\ \bar{1}]_B$). (b) Synergetic advancement of the (1 1 $\bar{1}$) ledges results in the migration of the irrational (0.7205 1 $\bar{1}$) twin boundary, leading to the growth of one variant at the expense of the other (viewed along $[0\ 1\ \bar{1}]_{A,B}$).

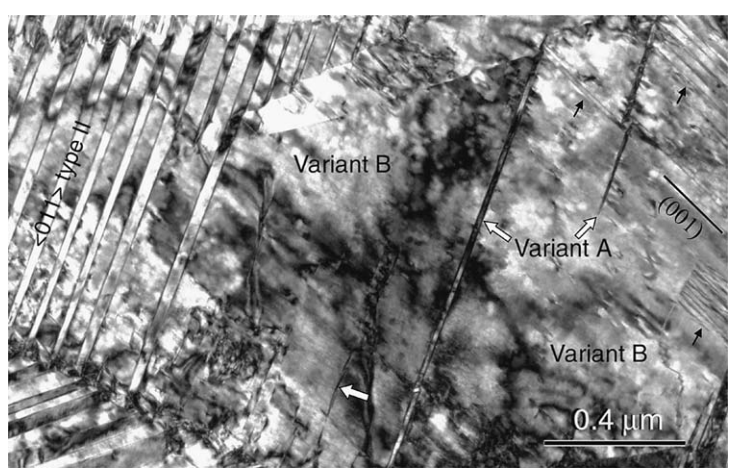

Fig. 10. Detwinning of ⟨0 1 1⟩ type II twin in NiTi sheet after 6% tension deformation along rolling direction. **B**//$[1\ 0\ 1]_A$//$[\bar{1}\ 1\ 0]_B$ in twinned area, and **B**//$[\bar{1}\ 1\ 0]$ in detwinned area.

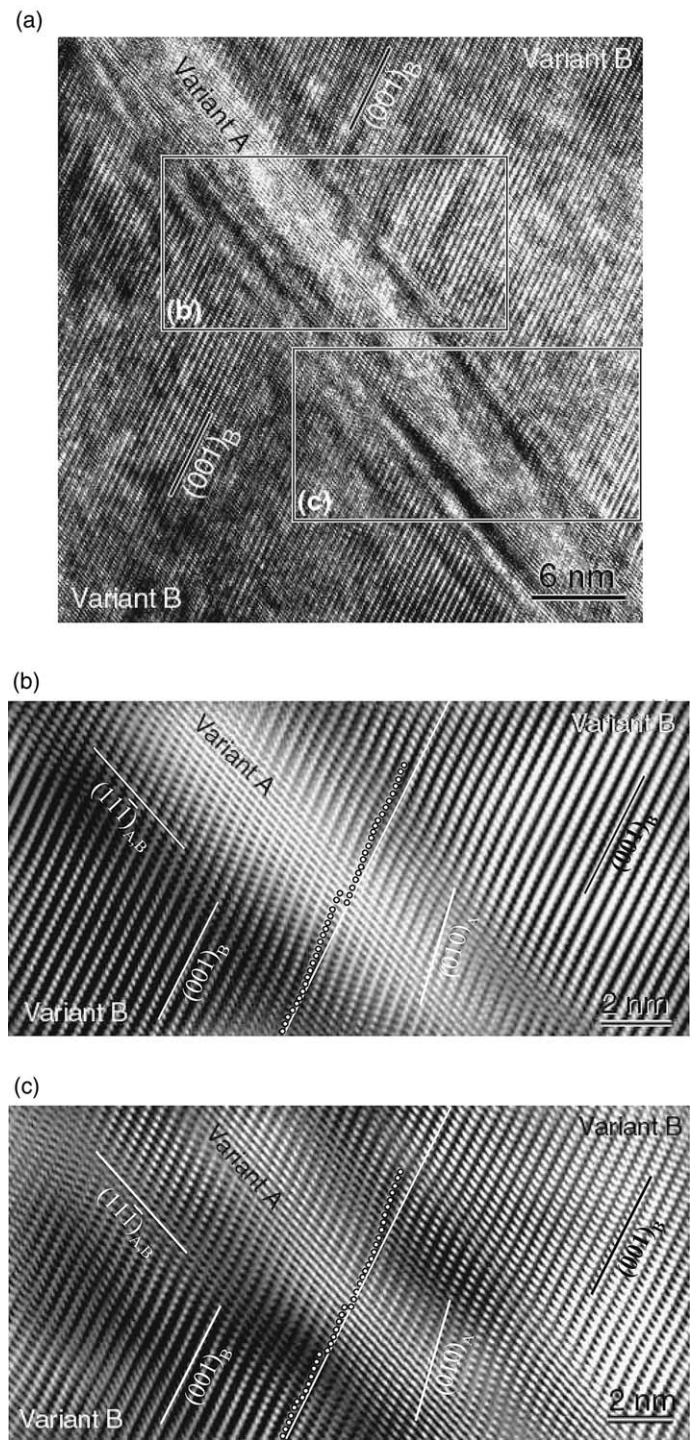

Fig. 11. (a) HREM micrograph of the detwinning region of $\langle 0\,1\,1\rangle$ type II twin. IFFT images (b, c) corresponding to the framed areas (b, c) in (a).

matically shown in Fig. 9. The atomic shear on the (1 1 $\bar{1}$) plane results in the advancement of (1 1 1) ledges along their normal directions (Fig. 9a). A synergetic movement of the (1 1 $\bar{1}$) ledges leads to the migration of the irrational twin plane (0.7205 1 $\bar{1}$), leading to the growth of one variant at the expense of the other (Fig. 9b). Such mechanism can be used to account for the "macroscopic" observations [19].

3.5. HREM observation of detwinning

The above detwinning model was further verified experimentally. When a NiTi martensite is deformed under tension to 6%, some of the martensite twins were detwinned, as typically shown in Fig. 10. In this observed area, both twinned and detwinned martensite variants coexist. In the twinned region, several ⟨0 1 1⟩ type II twin bands are clearly visible. Confirmed by the electron diffraction analysis, the neighbouring martensite variants are orientated in $[1\,0\,1]_A//[1\,1\,0]_B$ directions. In the other regions, mainly martensite variant B exists, while variant A became very narrow and was nearly vanished, as indicated by white arrows. As a result of detwinning, variant B grew significantly at the expense of the variant A. In addition, some black traces parallel to (0 0 1) plane are visible in the detwinned area as indicated by the black arrows. They are believed to be planar defects formed during detwinning process [25].

The atomic arrangement of a nearly detwinned area was further studied by using HREM and is shown in Fig. 11a. The observation direction is the same as that of Fig. 10, i.e., electron beam was parallel to $[1\,0\,1]_A//[\bar{1}\,1\,0]_B$. The variant A in between the two variants B nearly disappeared after the deformation. The migration of twin boundary results in a strain contrast along the boundary, and the boundary is still locally parallel to (1 1 $\bar{1}$) plane. The detailed atomic configuration of detwinning area can be seen in Figs. 11b and 11c, which are the IFFT images corresponding to the two framed regions in Fig. 11a. As is visible, in the whole detwinning area, all the (1 1 $\bar{1}$) planes are still parallel to each other and no distortion of (1 1 $\bar{1}$) plane is visible. This suggests that the atomic shear was in the (1 1 $\bar{1}$) plane. Between the two variants B, the (0 1 0) plane of variant A is reoriented, on the way to be aligned with $(0\,0\,\bar{1})_B$ via atomic shear on (1 1 $\bar{1}$) planes. This observation confirms the detwinning mechanism of ⟨0 1 1⟩ type II twin proposed in the present study (Fig. 9).

4. Conclusions

The ⟨0 1 1⟩ type II twin in NiTi SMA was investigated through crystallographic analysis and by means of HREM. Present results show that the irrational twin plane of (0.7205 1 $\bar{1}$) is composed of rational (1 1 1) ledges that are the atomic-scaled twin plane of the ⟨0 1 1⟩ type II twin. Based on the proposed model and supported by the experimental observations, the detwinning of ⟨0 1 1⟩ type II twin is achieved through the atomic shear along [0 1 1] direction in (1 1 $\bar{1}$) plane. A synergetic advancement of the rational (1 1 $\bar{1}$) ledges results in the migration of the irrational (0.7205 1 $\bar{1}$) twin boundary, leading to the growth of one variant at the expense of the other.

References

[1] Funakubo H. Shape memory alloys. New York: Gordon and Breach Science Publishers, 1984.
[2] Duerig TW, Melton KN, Stöckel D, Wayman CM. Engineering aspects of shape memory alloys. London: Butterworth-Heinemann, 1990.
[3] Otsuka K, Wayman CM. Shape memory materials. London: Cambridge University Press, 1998.
[4] Yahia L. Shape memory implants. Germany: Springer-Verlag, 2000.
[5] Van Humbeeck J. Mater Sci Eng A 1999;A273-A275:134.
[6] Duerig T, Pelton A, Stöckel D. Mater Sci Eng A 1999;A273-A275:149.
[7] Knowles KM, Smith DA. Acta Metall 1981;29:101.
[8] Otsuka K, Sawamura T, Shimizu K. Physica Status Solidi 1971;5:457.
[9] Gupta SP, Johnson AA. Trans Jpn Inst Metals 1973;14:292.
[10] Christian JW. Theory of transformations in metals and alloys. Oxford: Pergamon Press, 1965.
[11] Knowles KM. Phil Mag 1982;A45:357.
[12] Nishida M, Yamauchi K, Itai I, Ohgi H, Chiba A. Acta Metall Mater 1995;43:1229.
[13] Michal GM, Sinclair R. Acta Crystallogr 1981;B37:1803.

[14] Liu Y, Xie ZL, Van Humbeeck J, Delaey L. Acta Mater 1999;47:645.
[15] Liu Y, Xie ZL, Van Humbeeck J, Delaey L, Liu YN. Phil Mag 2000;A80:1935.
[16] Hehemann RF, Sandrock GD. Scripta Metall 1971;5:801.
[17] Kudoh Y, Tokonami M, Miyazaki S, Otsuka K. Acta Metall 1985;33:2049.
[18] Xie ZL, Liu Y. THERMEC-2003. International Conference on Processing and Manufacturing of Advanced Materials, July 2003, Madrid, Spain, 2003;426-432:2291-6.
[19] Miyazaki S, Otsuka K, Wayman CM. Acta Metall 1989;37:1885.
[20] Xie ZL, Liu Y, Van Humbeeck J. Acta Mater 1998;46:1989.
[21] Liu Y, Xie ZL, Van Humbeeck J, Delaey L. Acta Mater 1998;46:4325.
[22] Gall K, Sehitoglu H, Anderson R, Karaman I, Chumlyakov YI, Kireeva IV. Mater Sci Eng A 2001;317:85.
[23] Sehitoglu H, Hamilton R, Canadinc D, Zhang XY, Gall K, Karaman I et al. Metall Mater Trans A 2003;34(1):5.
[24] Kelly A, Groves GW, Kidd P. Crystallography and crystal defects. John Wiley & Sons, 2000.
[25] Xie ZL, Liu Y. Phil Mag, submitted.